PERGAMON

International Journal of Heat and Mass Transfer 46 (2003) 237–249

International Journal of HEAT and MASS TRANSFER

www.elsevier.com/locate/ijhmt

Film cooling characteristics of a single round hole at various streamwise angles in a crossflow Part II: heat transfer coefficients

C.H.N. Yuen [1], R.F. Martinez-Botas *

Department of Mechanical Engineering, Imperial College of Science, Technology and Medicine, London SW7 2BX, UK

Received 16 November 2001; received in revised form 19 July 2002

Abstract

Measurements of heat transfer coefficient (h) are presented for single jets with streamwise angles of 30°, 60° and 90° with a short but engine representative hole length ($L/D = 4$). The freestream Reynolds number (Re_D) is 8563, and the blowing ratio (M) ranges from 0.33 to 2. The results are presented in the form of h/h_0 which is the ratio of heat transfer coefficient with film cooling to that without. Both local values and laterally averaged ones are presented, the latter refers to the averaged value across the central hole. The corresponding measurements of effectiveness are presented in a companion paper [C.H.N. Yuen, R.F. Martinez-Botas, Int. J. Heat Mass Transfer, Part I]. In general, only slight variations in h/h_0 occurred as the blowing ratio was increased with the single 30° hole, in some contrast to the corresponding effectiveness measurements presented in the companion paper [Yuen and Martinez-Botas, Part I]. The single 60° and 90° jets yielded a smaller heat transfer coefficient than the 30° jet.

1. Introduction

The turbine entry temperature has almost doubled over a period of 25 years as a result of high temperature-rise combustors for greater specific thrust. However, the material turbine blades are made of, cannot withstand such high temperatures and has to be cooled substantially in order to achieve the required life span under such adverse centrifugal and thermal stress levels, therefore it is essential to improve cooling designs to keep the temperature level and thermal gradients in various turbine components within acceptable limits. Film cooling provides thermal protection to the blade metal wall and downstream of the holes by means of injection of cooler air over the external surface, forming an insulating layer between the hot main flow and the surface to be cooled, thereby reducing the heat transfer to the surface.

Aerodynamic and thermal procedures currently available to turbine designers have deficiencies that do not permit a priori designs that achieve design goals without expensive development iterations. The current study aims to construct a comprehensive set of results starting with a single round hole with the same operating conditions in the same test facility with wide band liquid crystal thermography and the steady-state heat transfer technique, which is much anticipated in the construction of reliable correlations for the application of film cooling in gas turbine industries.

Studies of isothermal heat transfer with film cooling (using jets at the same temperature as the freestream) on streamwise directed holes on a flat plate shown in Fig. 1, have been carried out by researchers such as Eriksen and Goldstein [2]; Goldstein and Yoshida [3]; Hay et al. [4]; and Ammari et al. [5]. Similar studies using heated or cooled jets have been done by Loftus and Jones [6] and Ligrani et al. [7]. Ligrani et al. [8], Schmidt et al. [9] and

* Corresponding author. Tel.: +44-20-75947241; fax: +44-20-78238845.

E-mail address: r.botas@ic.ac.uk (R.F. Martinez-Botas).

[1] Present address: ESDU International, London N1 6UA, UK.

0017-9310/03/$ - see front matter © 2002 Elsevier Science Ltd. All rights reserved.
PII: S0017-9310(02)00273-9

Nomenclature

A/D	analogue to digital
AMG	American gage
D	hole diameter
h	heat transfer coefficient in the presence of film cooling (W/m^2 K) $h = q''/(T_w - T_{aw})$, where T_{aw} is substituted by T_∞ when $T_2 = T_\infty$
h_0	heat transfer coefficient in the absence of film cooling (W/m^2 K) $h_0 = q''/(T_{w0} - T_\infty)$
HSI	hue, saturation, intensity
L	hole length
M	blowing ratio ($\rho_2 U_2/\rho_\infty U_\infty$)
q''	wall heat flux (W/m^2)
Re_D	Reynolds number ($\rho_\infty U_\infty D/\mu_\infty$)
RGB	red, green and blue
SWG	standard gage
T	temperature (K)
TLC	thermographic liquid crystals
U	velocity (m/s)
X	coordinate: streamwise (axial) direction (see Fig. 4)
Y	coordinate: vertical (heightwise) direction (see Fig. 4)
Z	coordinate: lateral direction

Greek symbols

δ	boundary layer thickness
δ^*	displacement thickness $\delta^* = \int_0^\delta (1 - (U/U_\infty))\,dy$
δ_i	momentum thickness $\delta_i = \int_0^\delta (1 - (U/U_\infty))U/U_\infty\,dy$
ρ	density (kg/m^3)

Subscripts

∞	freestream
0	in the absence of film cooling
2	coolant or secondary injection
aw	adiabatic wall
w	wall
Overbar	laterally averaged

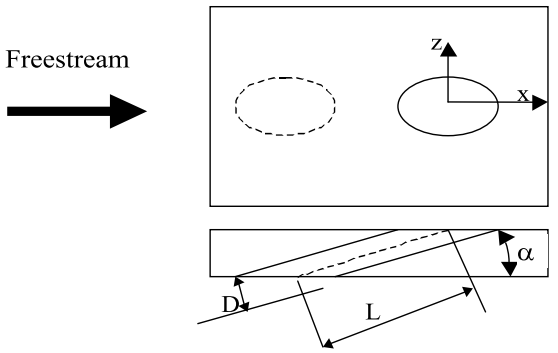

Fig. 1. Hole at an streamwise angle, α.

Sen et al. [10] showed it is important to have information of the film cooling effectiveness and the heat transfer coefficient. The non-dimensional centreline heat transfer coefficient increased by as much as 40–50% near the holes due to the presence of the streamwise vortices, compared to that in the absence of film cooling. Heat transfer coefficient downstream of a single hole increased with increasing blowing ratio, because once the jet started to lift off, the pressure deficit caused the freestream to enter the region below the jet, and increased the heat transfer rate locally.

Burd and Simon [11,12], Brundage et al. [13] and Walters and Leylek [14] found that the hole length was significant in determining the exit conditions for a single row of 35° holes with a length-to-diameter ratio of 3.5, and that the short holes were subject to skewed jet velocity profiles, such that a maximum velocity occurs in the downstream half of the hole, and it is larger than that of a turbulent jet for the same mass flow hole with low blowing ratios. This non-uniform velocity distribution of the exiting jet is referred to as jetting hereafter, and it depends on the hole geometry and the blowing ratio.

Lloyd and Brown [15] concluded that short holes may give rise to greater heat transfer than longer holes. Andrews et al. [16] independently concluded that large length-to-diameter ratios decreased the Nusselt number at a constant Reynolds number for 90° holes with a range of length-to-diameter ratio from 4.85 to 9.92. Cho and Goldstein [17] varied the hole length-to-diameter ratio from 0.68 to 1.5, and found that the region around the exit of a short hole was directly influenced by the crossflow.

The definition of heat transfer coefficient, h, is given in the Nomenclature. The objective of film cooling is to achieve low heat transfer from the surrounding hot mainstream to the turbine blades, and large effectiveness on the blade surface. The interpretation of wall measurements of temperature such as these reported in this paper benefits from knowledge of local velocities and wall pressures reviewed in Yuen and Martinez-Botas [1], and will not be repeated here.

2. Experimental apparatus and procedure

2.1. Liquid crystal thermography

Baughn [18] reviewed methods of involving narrow band crystals and wide band liquid crystals for measurements of local heat transfer coefficients with both the steady state and transient state techniques. Numerous studies using liquid crystal thermography have been described in Yuen and Martinez-Botas [1], and will not be repeated here. In the present study, wide band crystals and the steady-state heat transfer method are implemented. The details of this technique are provided in Yuen [19]. The encapsulated liquid crystal used in current study supplied by Thermax Ltd. [2] offers a bandwidth of 10 °C.

2.2. Test facility

Fig. 2 shows a schematic of the test rig of modular design. The test section comprised of a knife bleed, an injection plate and a test plate with a constant heat flux, the details of which are described in the following paragraphs. The roof and the side windows of the working section were made of Perpsex, which allowed optical access for the imaging system and thermal insulation.

A 40 mm long aluminium plate with a 45° chamfer at the upstream end, referred to as the knife bleed, spanned across the width (360 mm) of the test section, was designed to control the origin of the freestream boundary layer in the test section. It was made of stainless steel because it could be easily machined to produce a sharp knife-edge as well as being durable. The gap between the knife and the contraction lip could be adjusted by axial and vertical traverse mechanisms in the support frame, and the gap could be closed completely should no bleeding be desired. A 20 mm wide sandpaper was adhered onto the knife bleed at 35 mm from the chamfered end in order to trip the freestream boundary layer.

A 225 mm long injection plate spanned across the width of the test section, 360 mm, and was designed to be interchangeable with other plates with different cooling hole geometries. Three injection plates were made of Perspex, and each plate contained two rows of nine cylindrical holes of the same inclination. The centre hole in the downstream row was used whilst the other holes were covered with thin tape. The holes were positioned as close as possible to the downstream edge of the injection plate, such that the trailing edge of the holes was 6 mm from the downstream edge of test plate, which was desirable from the view point of measurements. This location was compromised by the space required for the plenum chambers underneath the injection plate.

Immediately downstream of the injection plate was the composite test plate, 360 mm wide by 1000 mm long by 163 mm thick, which was designed to deliver a constant heat flux (Fig. 3). Table 1 summarises the layers of the composite heater plate. It comprised of a 0.2 mm thick stainless steel sheet adjacent to the flow, used as the convective heat transfer test surface, and was heated from underneath by 18 (0.08 mm thick) Inconel strips (54 mm wide in the streamwise direction), which spanned across the entire width of the test plate. The heating elements were arranged in a serpentine fashion with a 1 mm gap between adjacent strips, and they were electrically connected in series by 3 mm thick copper bus bars on either side. The gap between the adjacent heater strips was kept as narrow as possible to reduce the periodic heat flux variation in the streamwise direction, but wide enough to allow for installation of thermocouples. Typical gaps between the adjacent metal strips used in heater plate construction were 0.04 mm by Goldstein and Yoshida [3], 0.25 mm by Mick and Mayle [20] and 1 mm by Sen et al. [10].

The 0.2 mm thick silicon impregnated sheet was sandwiched between the stainless steel sheet and the Inconel strips to provide electrical insulation, and at the same time, promote heat conduction to the test surface. The Inconel strips were adhered to the 10 mm thick Tufnol sheet (kite brand) with good thermal resistance and mechanical strength. Two 10 mm wide slots were milled into the two longer sides of the Tufnol plate to accommodate for the copper bus bars which were mounted flushed by countersunk screws, to ensure a flat surface (Fig. 3). A 150 mm thick extruded polystyrene (styrofoam) block was epoxied beneath the Tufnol plate to reduce further heat loss, and was followed by a 3 mm thick sheet of mild steel to support the entire composite block.

The reasons that this heating arrangement, was selected rather than (a) passing current through the stainless steel foil, such that the foil itself is the heater, like that used by Rastogi [21]; and (b) using the serpentine-Inconel strips directly as test surface like that used by Goldstein and Yoshida [3], Sen et al. [10], Mick and Mayle [20] and Eriksen [22], and are the current required by method (a) is larger, furthermore a large thin metal surface is prone to have non-uniform resistance which would result in uneven heat flux distribution; the heat flux delivered by method (b) is further from the ideal constant one than that proposed by method (a). Therefore, a compromise between the two commonly used construction methods was reached, the main purpose of the extra layer of stainless steel foil and silicon impregnated sheet is to reduce the periodic heat flux generated by the serpentine heater strips, and

[2] Thermax (Thermographic Measurements Ltd.), Bank House, Neston Road, Burton, South Wirral L64 5TA, England.

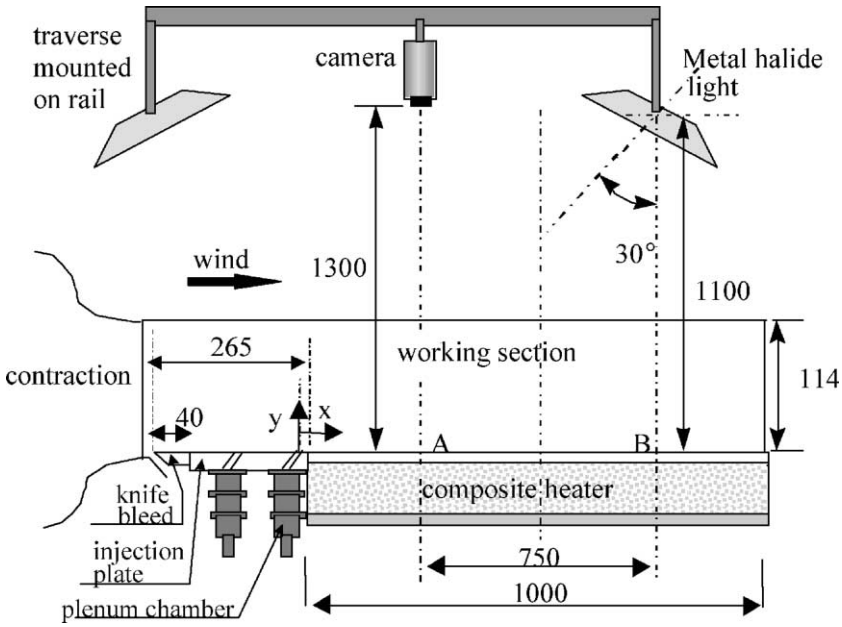

Fig. 2. Experimental set-up.

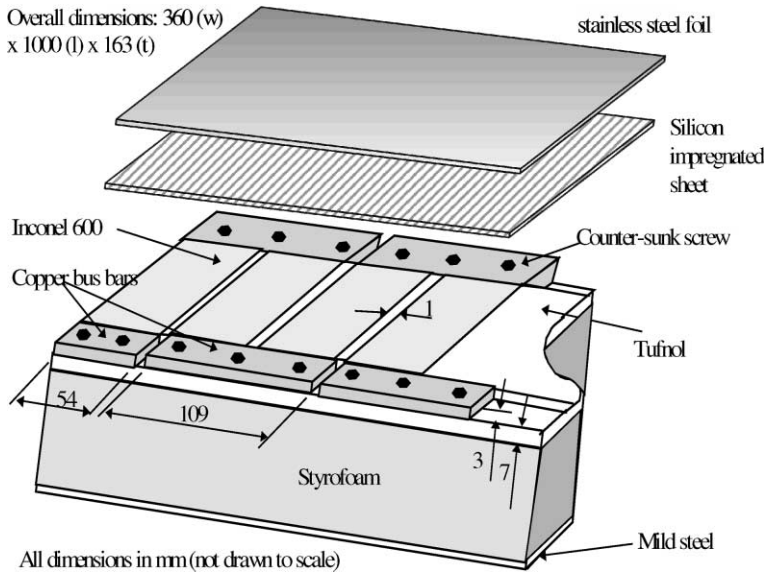

Fig. 3. Test plate with a constant heat flux.

minimise any non-uniformity inherent in the heat flux distribution. Such combination was also used by Wang et al. [23] and Ligrani and Williams [24]. Ten T-type (copper–constantan) American gage 36 (SWG 39–40) thermocouples were installed in the composite test plate.

A single phase transformer with two 25 V r.m.s secondary windings running at 35 A was especially made to power the heating elements, and was controlled by a variac. Two small probes were used to measure the voltage drop between two points 1 cm apart along the Inconel strips to check uniformity in resistance, before the uppermost layer of stainless steel sheet was mounted, and the result was satisfactory. The uniformity of heat flux was further verified when the convective surface was coated with thermographic liquid crystals, and heated at

Table 1
Materials in the test plate

Order	Materials	Thermal conductivity (W/mK)	Functions
Top	0.2 mm stainless steel 304 Foil	14.9	Convective heat transfer surface
	0.2 mm thick silicon impregnated sheet	0.79	Thermal conductance Electrical insulation
	0.08 mm thick Inconel 600	14.8	Heating element
	10 mm Tufnol (kite brand)	0.26	Thermal insulation Mechanical support
	15 cm styrofoam	0.027	Thermal insulation
Bottom	3 mm mild steel	60	Mechanical support

different electrical settings, the standard deviation of hue displayed was within one unit (out of 256) in the vicinity of the thermocouples, and on the entire test plate.

The laboratory compressed air was filtered, regulated by a needle valve and monitored by a rotameter before entering an inline pipe heater, the plenum chamber and, finally, the injection plate. A flow straightener was inserted into the straight pipe section just upstream of the rotameter. The jet temperature was measured by a T-type (copper-constantan) thermocouple of American gage 36 at the cooling hole entrance, and the temperature was 20 ± 0.1 °C approximately. The temperature was checked at the hole exit to ensure that the temperature loss across the hole was negligible.

2.3. Image processing and calibration

The imaging system used is identical to that used in Yuen and Martinez-Botas [1]. It comprised of a colour JVC CCD camera, two light sources, and a 24-bit frame grabber installed in a computer. The test section was contained in a spacious tent made of anti-flammable black cloth to eliminate variations in illumination, such as the time of day, and was sufficiently large for air circulation. The temperature and hue calibration process for the liquid crystals and the data reduction method used are the same as those employed in Yuen and Martinez-Botas [1].

2.4. Experimental uncertainty

Uncertainties are evaluated by the method of Kline and McClintock [25]. Corrections are applied to consider heat loss through thermocouple leads using the method proposed by Schneider [26]. Corrections for radiation from the heated test surface coated with liquid crystals and conduction out the back of the test surface are included into the analysis, such that subtraction of these corrections from the average heat generated within the heater gives the net local heat flux. The uncertainty in h/h_0 is approximately $\pm 7\%$.

2.5. Operating conditions

The freestream Reynolds number based on the hole diameter and freestream velocity, Re_D, was 8563. The freestream velocity, temperature and turbulence intensity were 13 m/s, 20 °C and 2.7% respectively. The injectant-to-freestream blowing ratio varied from 0.33 to 2. The heat transfer tests were conducted with a constant heat flux of 410 W/m^2 and with the injectant at 20 °C ($\rho_2/\rho_\infty = 1$). The jet temperature was measured by a T-type thermocouple at the hole exit and in the plenum chamber. The injectant temperature refers to that at the hole exit. The test cases investigated in the current study are listed in Table 2. Table 3 provides the boundary layer characteristics.

Table 2
Test cases

Configuration	Streamwise angles	Hole length (L/D)	Blowing ratio (M)	Re_D
Single hole	30°, 60° and 90°	4	0.33, 0.5, 0.67, 1.0, 1.33, 1.67 and 2.0	8563

Table 3
Boundary layer characteristics

Position	Boundary layer thickness (δ/D)	Displacement thickness (δ^*/D)	Momentum thickenss (δ_i/D)
Injection plane ($x/D = 0$)	1	0.15	0.11

3. Results

In the results presented here, the axial range is classified into four regimes for clarity: the immediate region for $x/D \leqslant 3$, the near field for $3 \leqslant x/D \leqslant 7$, the intermediate region for $7 \leqslant x/D \leqslant 26$, and the far downstream region for $x/D \geqslant 26$.

3.1. Hole with 30° injection angle

Fig. 4(a)–(g) displays the contours of non-dimensional heat transfer coefficient, h/h_0, with a single 30° hole and blowing ratios in the range from 0.33 to 2. The direction of crossflow is from left to right, the origin of the axial distance, x/D, and lateral distance, z/D, commence from the centre of the cooling hole, as shown in Figs. 1 and 2. The value of 1.55 was achieved in the immediate region, and decreased with downstream distance since the mixing underneath the jet and at its edge was large. The increase in local mixing resulted in high heat transfer from the heated wall to the ambient surroundings and, thus the h/h_0 value.

The heat transfer coefficient in the immediate region was approximately 1.6 times that without film cooling. The region of heat transfer coefficient greater than 1.1 elongated from x/D of 9 to x/D of 26 approximately with a blowing ratio of 0.33 and 2 respectively. In general, only slight variations in h/h_0 occurred as the blowing ratio was increased with the single 30° hole, in some contrast to the corresponding effectiveness measurements presented in the companion paper [1].

Fig. 5(a)–(g) presents the non-dimensional heat transfer coefficient at z/D of 0, 0.44, 1.1, 1.55 and 1.77, and since symmetry has been demonstrated in Fig. 4, is confined to positive lateral positions. The centreline heat transfer coefficient in the vicinity of injection with a blowing ratio of 0.33 in Fig. 5(a) was approximately 55% higher than that without blowing. It reduced to nearly unity for $x/D > 13$, and the more interesting features lie close to the hole. The maximum value of 1.78 was not on the centreline, but at z/D of 0.44, which suggests that the flow underneath the core of the jet was more turbulent towards its edges, where the shear with the freestream was large. The rate of decrease in h/h_0

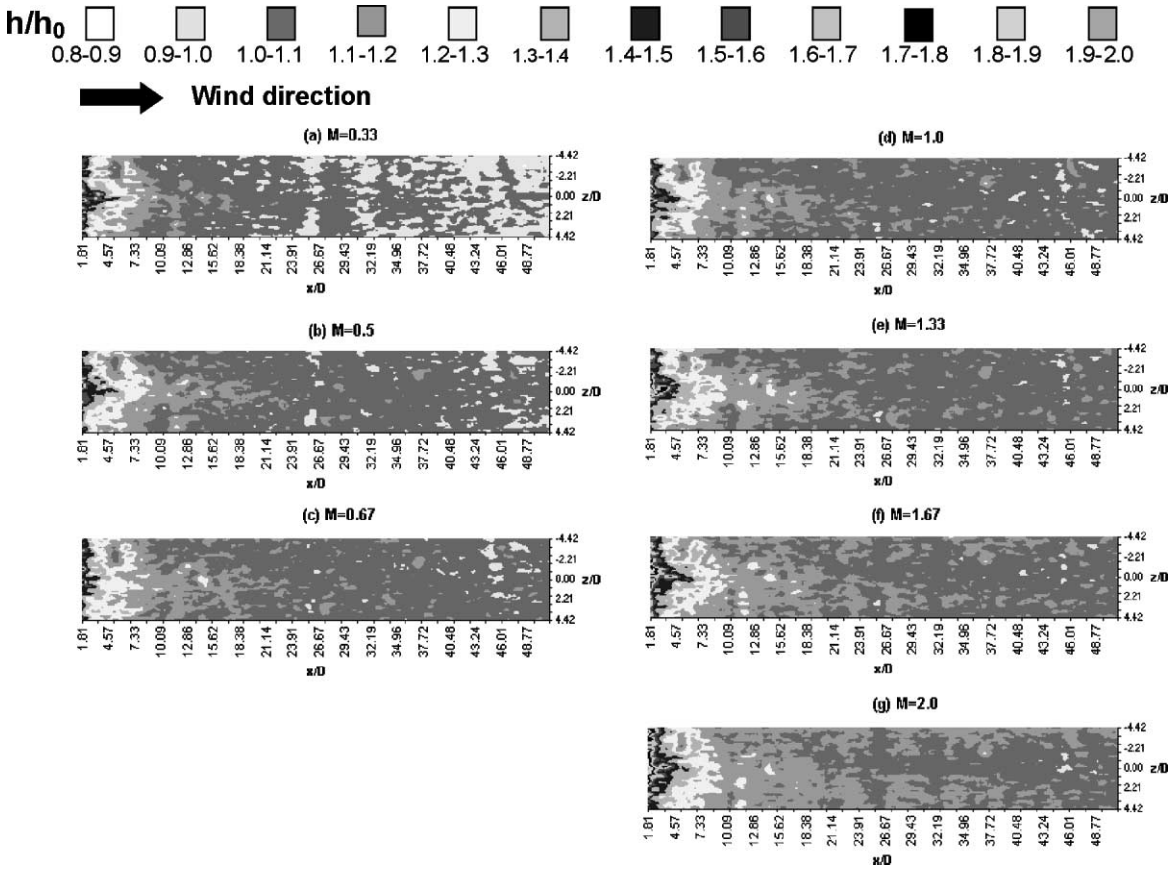

Fig. 4. Distribution of heat transfer coefficient, h/h_0, for a single 30° hole.

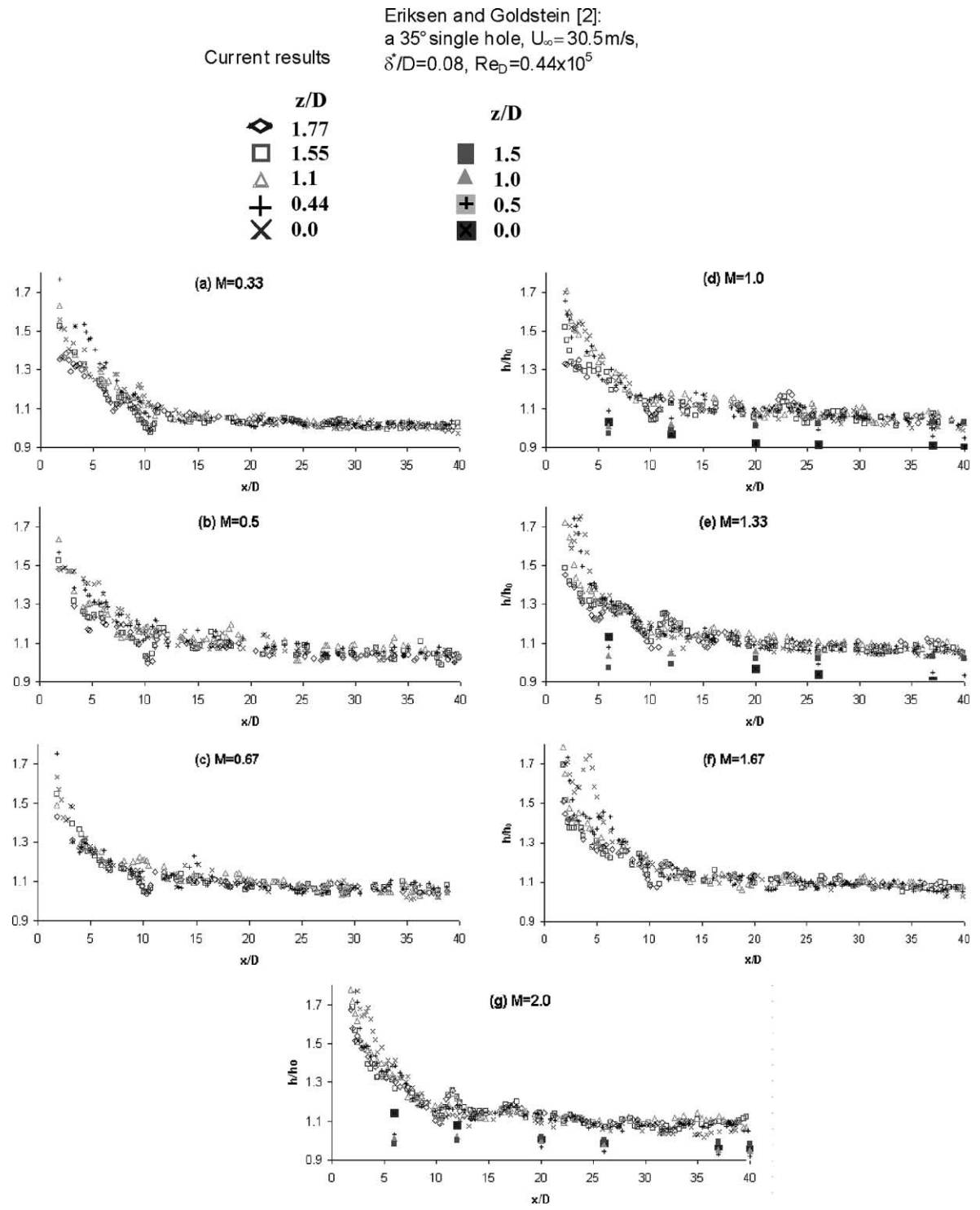

Fig. 5. Lateral distributions of h/h_0 for a single 30° hole.

with downstream distance in the immediate region was steeper at z/D of 0.44 than on the centreline, consistent with the decreasing influence of the jet. The value of 1.62 at z/D of 1.1 was smaller than that found at z/D of 0.44

(h/h_0 of 1.78), but was still higher than that at the centreline ($h/h_0 \approx 1.55$) at the same downstream distance, and the values were similar for the immediate and near field regions at z/D of 1.55 and 0. A low value was recorded at x/D of 10 and z/D of 1.55 approximately, which was also observed at z/D of 1.77 at the same streamwise location, this showed that the lateral spreading of the jet reached approximately 1.8 times the hole diameter. The larger value of h/h_0 at finite radii compared to that found by Eriksen and Goldstein [2] perhaps suggests that the amount of disturbance added by the ejected jet was greater in the current study, which may be related to the lower level of effectiveness found in the companion paper [1].

The heat transfer coefficients were similar within one diameter of the hole in the lateral direction with blowing ratios greater than unity (Fig. 5(d)–(g)), and decreased with lateral distance in the near field, similar to that of Ammari et al. [5] who found high heat transfer coefficients at the edge of the jet at low blowing ratios, and large values on the centreline in the vicinity of the hole for intermediate and large blowing ratios. Fig. 5(d)–(g) showed how the peak value on the centreline at x/D of 3 shifted downstream as the blowing ratio was increased from unity to 1.33 and 1.67, and returned upstream with a blowing ratio of 2. This double shift may be induced by the variation in the mixing strength beneath the jet.

Also incorporated in Fig. 5(d) are the results of Eriksen and Goldstein [2] with a Re_D, δ^* and L/D of 44,000, 0.08 and 42.6 respectively, which may be compared to the current results with Re_D of 8563, δ^* of 0.15 and L/D of 4. Their results are generally lower than those found in the current measurements, the discrepancies could be caused by the differences in Re_D (almost 5-fold) and the length-to-diameter ratio (slightly more than 10-fold). They reported that the h/h_0 beyond z/D of unity increased with increasing downstream distance, which was not shown in the current results. However, they found that the maximum h/h_0 was located not on the centreline, but at the edge of the hole, similar to the current findings. It is questionable whether their scarce data points could be the reason for the absence of characteristics reported here, in their investigation.

The centreline h/h_0 was 1.75 times that without film cooling with a blowing ratio of 1.33 (Fig. 5(e)) in the near field. It can be seen more clearly that h/h_0 near the jet decreased as the lateral distance from the centreline was increased. Also included in this plot are the results of Eriksen and Goldstein [2] who found that the maximum h/h_0 in the proximity of the jet shifted from z/D and blowing ratio of unity to z/D of 0 with a blowing ratio of 1.33, consistent with the current results. The descending order of heat transfer coefficient was changed for blowing ratios greater than 1.67 (Fig. 5(e) and (f)), the maximum h/h_0 was no longer found at lateral locations, but on the centreline, and it decreased as z/D was increased, similar to the findings of Ammari et al. [5].

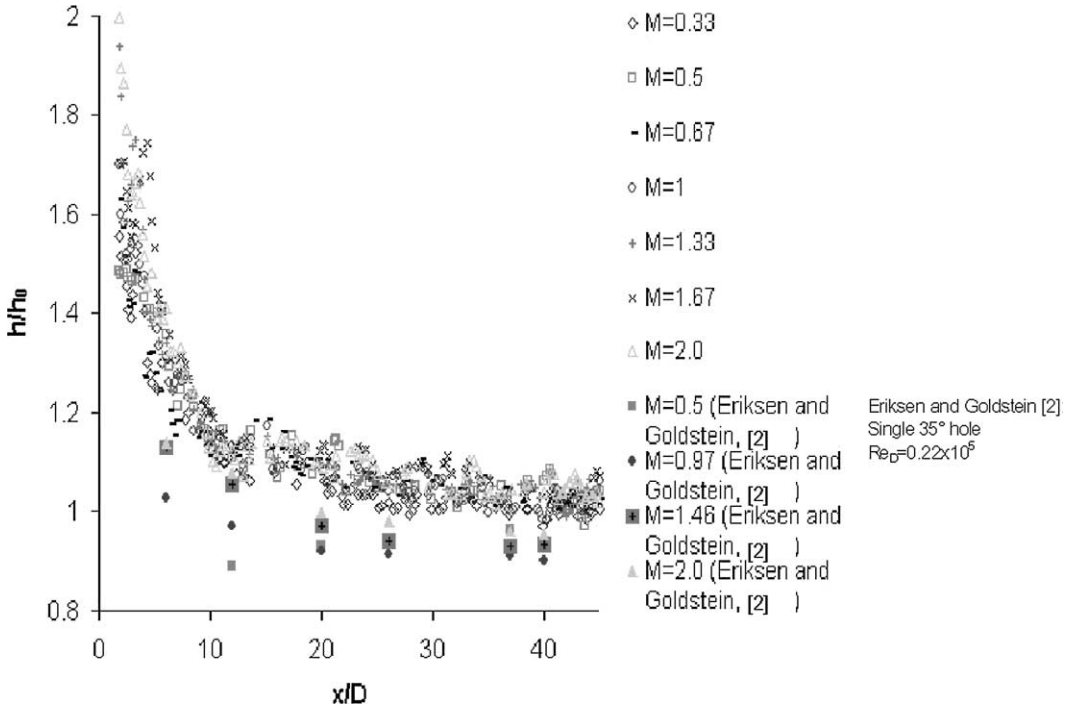

Fig. 6. Variations of centreline h/h_0 with streamwise distance for a single 30° hole.

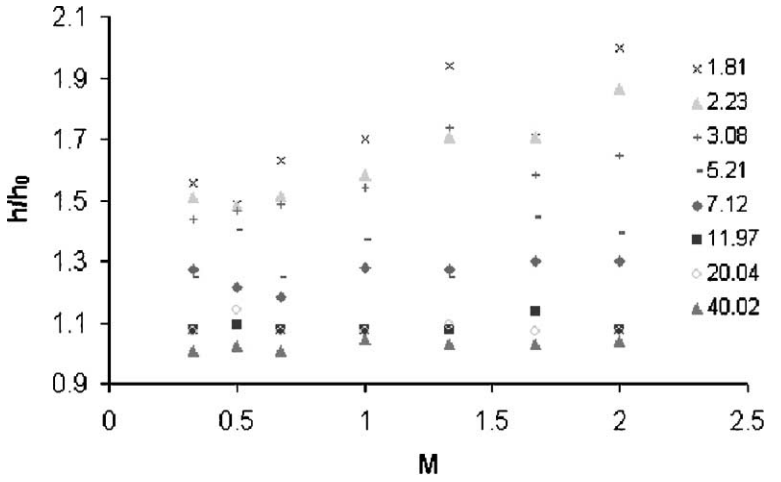

Fig. 7. Variations of centreline h/h_0 with blowing ratio for a single 30° hole.

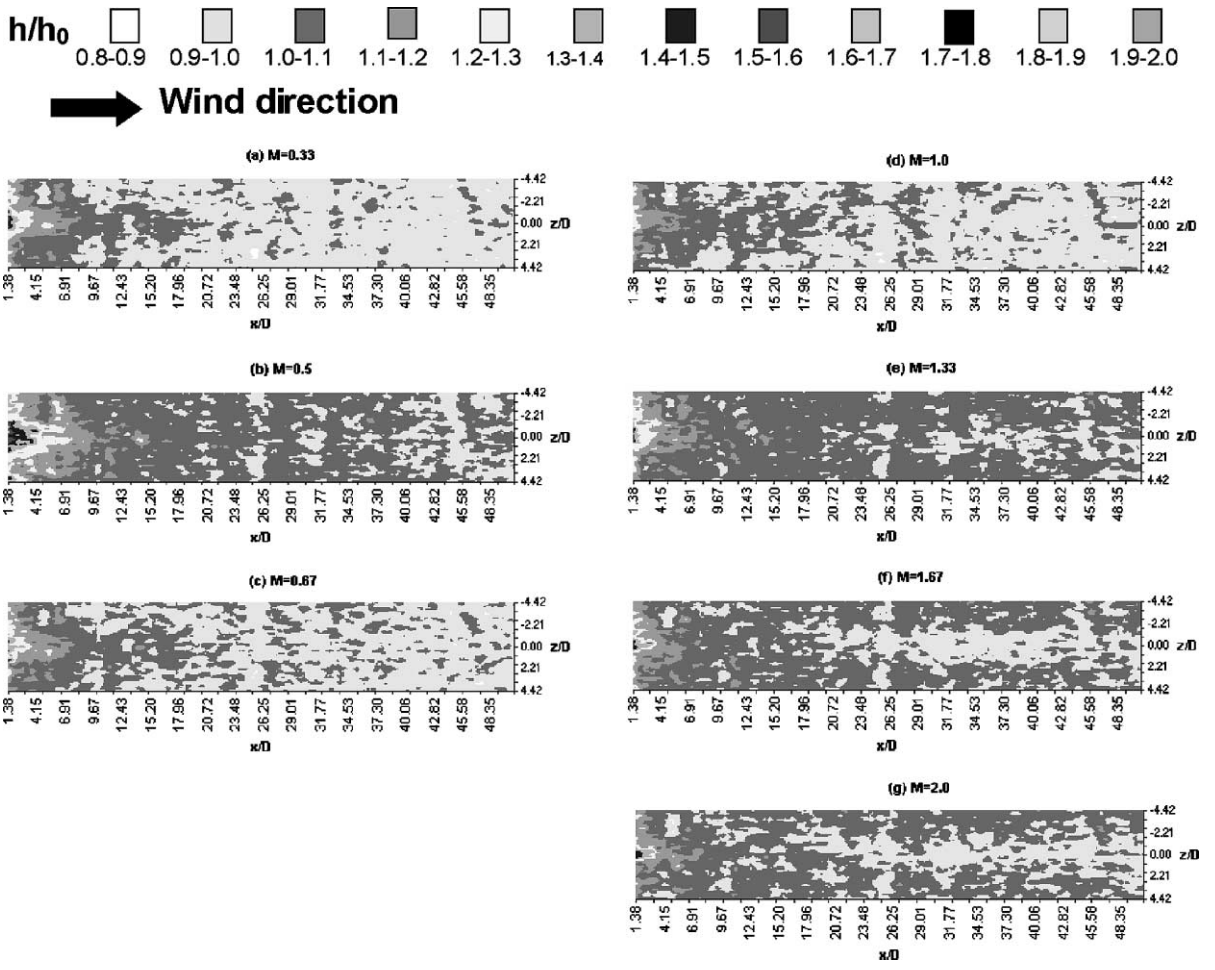

Fig. 8. Distribution of heat transfer coefficient, h/h_0, for a single 60° hole.

The normalised centreline heat transfer coefficient decreased from approximately 1.8 in the immediate and near field regions to 1.1 at x/D of 11 with a blowing ratio of 2 (Fig. 5(g)). The descending order of heat transfer coefficient with a blowing ratio of 2 and x/D of 6 found by Eriksen and Goldstein [2] was similar to that with a blowing ratio of 1.67 in Fig. 5(f), and that was z/D of 0, followed by 1.0 and 1.5. They also found that heat transfer coefficients at all lateral locations decreased to unity approximately further downstream, which is consistent with the current results.

Fig. 6 shows the effects of blowing ratio on the distribution of centreline h/h_0. The overall trend is for h/h_0 to decrease rapidly for the first 10 diameters downstream of the hole, decelerate and then to gradually increase to reach a plateau and decrease far downstream. There was little effect of blowing ratio on heat transfer in the vicinity of injection, when the maximum uncertainty was approximately 7% (see Section 2.4). In general, the larger blowing ratios produced greater h/h_0 values. It can be seen from Fig. 8 that the blowing ratios of 0.33 and 0.5 gave the lowest centreline heat transfer for all the axial locations measured. Also included in the figure are the results of Eriksen and Goldstein [2] who showed that the maximum heat transfer occurred with the blowing ratio of 1.95, followed by 1.46 and 0.97 for locations less than x/D of 27, consistent with the current findings. However, the gradual increase on the centreline h/h_0 with x/D at the blowing ratio of 0.5 was not found here, which may suggest that the mixing mechanism between the jet and its surrounding mainstream was very different.

Fig. 7 shows the distributions of centreline h/h_0 with blowing ratio for various axial locations. The blowing ratio had little influence on heat transfer except for the immediate and near field regions, where the centreline h/h_0 increased by approximately 25% as the blowing ratio was increased from 0.33 to 2.

3.2. Effects of jet angle

Figs. 8 and 9 present contours of non-dimensional heat transfer coefficients for the single 60° and 90° jets respectively. The single 60° jet yielded a smaller heat transfer coefficient than the 30° jet, in contrast to the findings of Goldstein and Eriksen [2].

As the 30° jet emerged from the hole, the shallow angle and the crossflow maintained the jet fluid closer to the wall than the steeper jets. The vortices described in the review in Yuen and Martinez-Botas [1] could entrain fluid from close to the wall, thus disturbing the local boundary layer, and as a result, producing higher level of

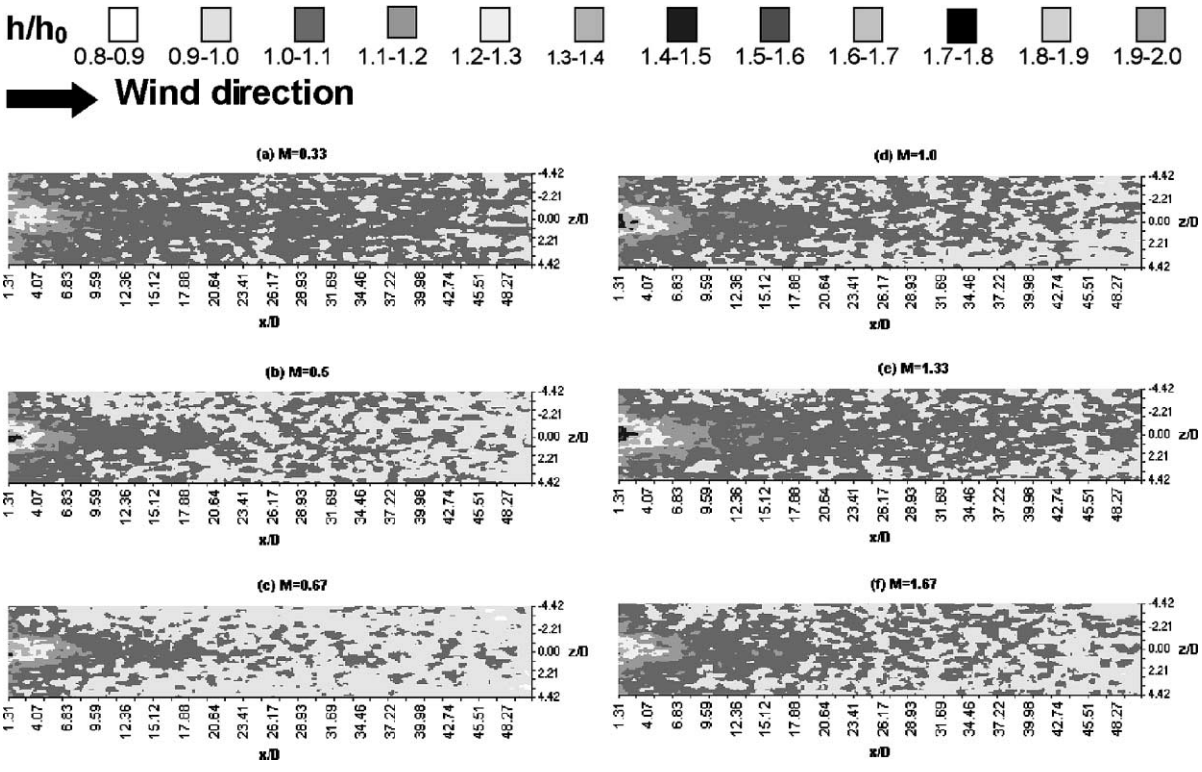

Fig. 9. Distribution of heat transfer coefficient, h/h_0, for a single 90° hole.

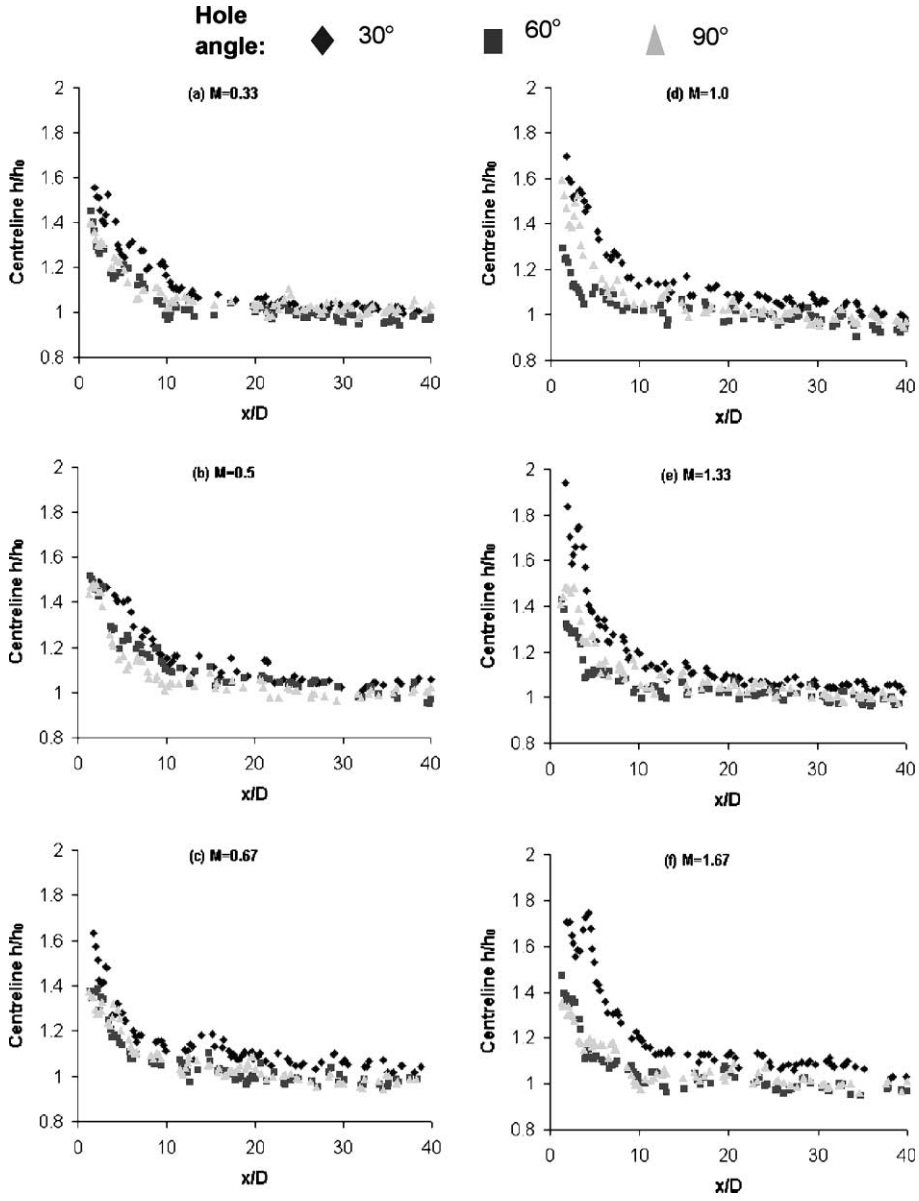

Fig. 10. Effects of streamwise angle on centreline heat transfer coefficient, h/h_0, for a single hole.

h/h_0 near the hole. It has been mentioned previously that jetting affected the distribution of fluid exiting the hole, and that the pressure distribution in the vicinity of the hole varied with streamwise angle, the 30° jet caused less disturbance upstream of the hole than the 90° jet. The 90° jet was further from the wall than the 30° jet at a given axial distance, thus the majority of the disturbances would be transported downstream by the crossflow and the dominant vortex pair, and these disturbances would be unlikely to propagate to the near wall region.

The trend of $h_{30^\circ} > h_{60^\circ} > h_{90^\circ}$ remained further downstream, $x/D \geqslant 10$. Ammari et al. [5] found similar behaviour downstream of his holes, but $h_{30^\circ} < h_{60^\circ} < h_{90^\circ}$ close to the holes, which is opposite to the present suggestion. This contradiction suggests that the flow structure in the near-hole region of the present flow may be very different. This near-jet flow field is complex, and the mechanism is not fully understood. The behaviour of the cooling film can change dramatically as the fluid mechanics of the film and the surrounding boundary layer are altered.

Figs. 10 and 11 present the variations of centreline and laterally averaged h/h_0 respectively with axial location for the three streamwise angles tested. The

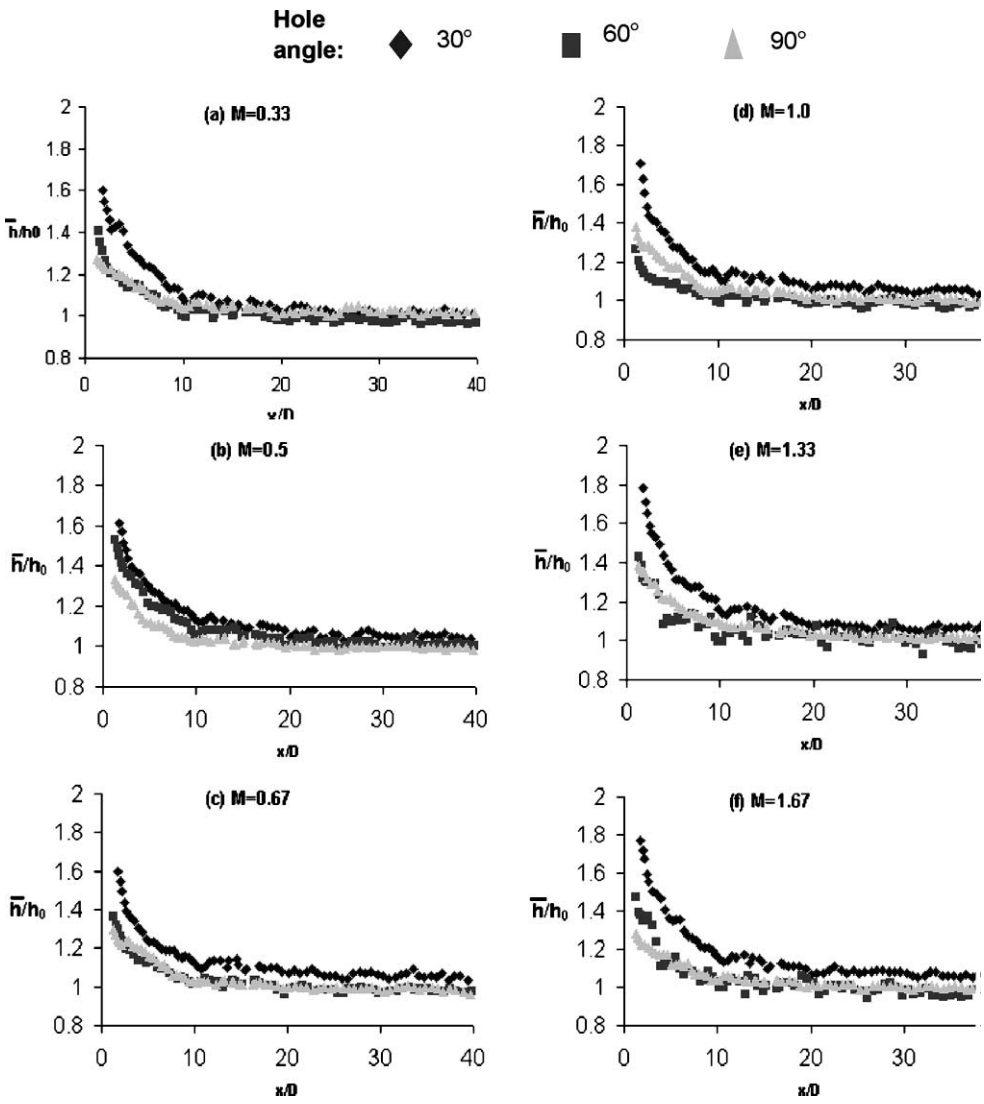

Fig. 11. Effect of streamwise angle on laterally averaged heat transfer coefficient, $\bar{h}/h_0$, for a single hole.

observation of the 30° jet imposing more disturbances close to the test wall is clearly shown for all blowing ratios on the centreline and at lateral positions.

4. Conclusions

1. In general, the blowing ratio had little influence on heat transfer except for the immediate and near field regions, where the centreline h/h_0 increased by approximately 25% as the blowing ratio was increased from 0.33 to 2.

2. The maximum h/h_0 value of 1.78 with a 30° hole and a blowing ratio of 0.33 was not on the centreline, but at z/D of 0.44, which suggests that the flow underneath the core of the jet was more turbulent towards its edges, where the shear with the freestream was large. The lateral spreading of the jet reached approximately 1.8 times the hole diameter. The larger values of h/h_0 at finite radii compared to that found by Eriksen and Goldstein [2] perhaps suggest that the amount of disturbance added by the ejected jets was greater in the current study, which may be related to the lower level of effectiveness in the companion paper [1].

3. The single 60° jet yielded a smaller heat transfer coefficient than the 30° jet. As the 30° jet emerged from the cooling hole, the shallow angle and the crossflow, maintained the jet fluid closer to the wall than the steeper jets. The vortices described could entrain fluid from close to the wall, thus disturbing the local boundary layer, and

as a result, producing higher level of h/h_0 near the hole. The pressure distribution in the vicinity of the hole varied with streamwise angle, and the 30° jet caused less disturbance upstream of the hole than the 90° jet. The 90° jet was further from the wall at a given axial distance compared to the 30° jet, the majority of the disturbances would be transported downstream by the crossflow and the dominant vortex pair, and these disturbances would be unlikely to propagate to the near wall region.

4. Further downstream, $x/D > 10$, the trend of $h_{30°} > h_{60°} > h_{90°}$ remained. Ammari et al. [5] found similar behaviour downstream of his holes, but found $h_{30°} < h_{60°} < h_{90°}$ close to the holes, which is opposite to the present suggestion. The behaviour of the cooling film can change dramatically as the fluid mechanics of the film and the surrounding boundary layer are altered. This highlights the importance of fluid mechanics in film cooling investigations.

Acknowledgements

The authors would like to thank Alstom Power Ltd., particularly Prof. J. Hannis, Dr. J. Turner, Dr. Gan for supporting the present work, and Thermax Ltd. for providing the liquid crystals.

References

[1] C.H.N. Yuen, R.F. Martinez-Botas, Film cooling characteristics of a single round hole at various angles in a crossflow: Part I—effectiveness, Int. J. Heat Mass Transfer 46 (2003), PII: S0017-9310(02)00274-0.

[2] V.L. Eriksen, R.J. Goldstein, Heat transfer and film cooling following injection through inclined circular tubes, ASME J. Heat Transfer (May) (1974) 239–245.

[3] R.J. Goldstein, T. Yoshida, Boundary layer and laminar injection on film cooling performance, ASME J. Heat Transfer 104 (1982) 355–362.

[4] N. Hay, D. Lampard, C.L. Saluja, Effects of cooling films on the heat transfer coefficient on a flat plate with zero mainstream pressure gradient, J. Eng. Gas Turbines Power 107 (1985) 105–110.

[5] H.D. Ammari, N. Hay, D. Lampard, The effect of density ratio on the heat transfer coefficient from a film-cooled flat plate, ASME J. Turbomach. 112 (1990) 444–450.

[6] P.J. Loftus, T.V. Jones, The effect of temperature ratios on the film cooling process, ASME J. Eng. Power 105 (1983) 615–621.

[7] P.M. Ligrani, A. Ortiz, S.L. Joseph, D.L. Evans, Effects of embedded vortices on film-cooled turbulent boundary layers, ASME J. Turbomach. 111 (1989) 71–77.

[8] P.M. Ligrani, S. Ciriello, D.T. Bishop, Heat transfer, adiabatic, effectiveness, and injectant distributions downstream of a single row and two staggered rows of compound angle film-cooling holes, ASME J. Turbomach. 14 (1992) 687–700.

[9] D.L Schmidt, B. Sen, D.G. Bogard, Film cooling with compound angle holes: adiabatic effectiveness, ASME J. Turbomach. 118 (1996) 807–813.

[10] B. Sen, D.L. Schmidt, D.G. Bogard, Film cooling with compound angle holes: heat transfer, ASME J. Turbomach. 118 (1996) 800–806.

[11] S.W. Burd, T.W. Simon, Measurements of discharge coefficients in film cooling, ASME Paper No. 98-GT-009, 1998.

[12] S.W. Burd, T.W. Simon, Turbulence spectra and length scales measured in film coolant flows emerging from discrete holes, ASME Paper No. 98-GT-190, 1998.

[13] A.L. Brundage, M.W. Plesniak, S. Ramadhyani, Influence of coolant feed direction and hole length on film cooling jet velocity profiles, ASME Paper No. 99-GT-35, 1999.

[14] D.K. Walters, J.H. Leylek, A detailed analysis of film cooling physics: Part I—streamwise injection with cylindrical holes, ASME J. Turbomach. 122 (2000) 102–112.

[15] S. Lloyd, A. Brown, Fluid flow and heat transfer characteristics in the entrance region of circular pipes, ASME Paper No. 85-GT-120, 1985.

[16] G.E. Andrews, M. Alikhanizadeh, A.A. Asere, C.I. Hussain, M.S. Khoshkbar, M.S. Azari, M.C. Mkpadi, Small diameter film cooling holes: wall convective heat transfer, ASME J. Turbomach. 108 (1986) 283–289.

[17] H.H. Cho, R.J. Goldstein, Heat (mass) transfer and film cooling effectiveness with injection through discrete holes: Part I—within holes and on the back surface, ASME J. Turbomach. 117 (1995) 440–449.

[18] J.W. Baughn, Liquid crystal methods for studying turbulent heat transfer, Int. J. Heat Fluid Flow 16 (5) (1995) 365–375.

[19] C.H.N. Yuen, Measurement of local heat transfer coefficient and film cooling effectiveness ion film cooling geometries, Ph.D. thesis, University of London, Imperial College of Science, Technology and Medicine, London, 2000.

[20] W.J. Mick, R.E. Mayle, Stagnation film cooing and heat transfer, including its effect within the hole pattern, ASME J. Turbomach. 110 (1988) 66–72.

[21] A.K. Rastogi, Effectiveness and heat transfer of three-dimensional film cooling slots, Ph.D. thesis, University of London, Imperial College of Science, Technology and Medicine, London, 1972.

[22] V.L. Eriksen, Film cooling effectiveness and heat transfer with injection through holes, Ph.D. thesis, University of Minnesota, 1971.

[23] T. Wang, T.W. Simon, J. Buddhavarapu, Heat transfer and fluid mechanics measurements in transitional boundary layer flows, ASME J. Eng. Gas Turbines Power 107 (1985) 1007–1015.

[24] P.M. Ligrani, W. Williams, Effects of an embedded vortex on injectant from a single film-cooling hole in a turbulent boundary layer, ASME J. Turbomach. 112 (1990) 428–436.

[25] S.J. Kline, F.A. McClintock, Describing uncertainties in single-sample experiments, Mech. Eng. (January) (1953) 3–8.

[26] P.J. Schneider, Conduction Heat Transfer, sixth ed., Addison-Wesley, Reading, MA, 1974, pp. 176–181.